Multi-Band RF Transceiver Based on the Polarization Multiplexed Photonic LOs and Mixers

Wenjuan Chen, Dan Zhu ⬩, *Member, IEEE*, Jiang Liu, and Shilong Pan ⬩, *Senior Member, IEEE, Fellow, OSA*

Abstract—A photonics-based multi-band RF transceiver is proposed and demonstrated. Both for the multi-band transmitter and receiver sections, the polarization multiplexed photonic LO unit is shared, and the dual-polarization photonic mixer modules with similar structures are introduced. The architectural complexity is reduced, bringing benefits to the reliability, dimensions, and cost of the system. Based on the same transceiver, RF signals in four bands can be simultaneously generated, and the RF echoes can be processed to the same IF band with the interference effectively suppressed. The strict requirements with either the photonic or the electrical filters are avoided. Furthermore, the generation and processing capability can be extended to being with 4*N* RF signals by introducing a polarization orthogonal optical frequency comb (OFC). The proposed architecture is therefore promising for the future cognitive radar systems which need to work in multiple bands and have a variety of functions to learn, infer, and react to the environment. A proof-of-concept experiment is taken. Four RF signals covering X, Ku, K and Ka bands with 1-GHz instantaneous bandwidth are simultaneously generated and processed. More than 26-dB crosstalk suppression ratio is realized for the four bands. The ranging operated in K- and Ka-bands simultaneously are also implemented.

Index Terms—Optical signal processing, transceivers, polarization, optical frequency conversion.

I. INTRODUCTION

COGNITION is considered to be one key enabling technology for the future radar systems working in the complex electromagnetic environment. In order to learn, infer and react to the environment, the cognitive radar systems are highly required to have a variety of functions, such as surveillance, tracking, imaging, and so on [1]–[4]. The optimized microwave working bands for diverse functions are different. For example, the early warning function is usually taken in the S band, the target tracking is commonly taken in the C and X bands, and the imaging funciton can be taken in the P, L, S, C, X and Ku bands

for a variety of applications [5], [6]. Thus the transceivers which can transmit and process multi-band signals are urgently needed. Due to the limitation in working frequency and bandwidth, the multi-band transceivers based on conventional electronic techniques are generally realized by using one set of devices for each working band [7], [8], leading to a great increase of the power, size, and weight of the system. Microwave photonics is a possible solution to realize multi-band transmitting and processing in one single transceiver, by taking advantages of ultrawide bandwidth, parallel processing, and immunity to electromagnetic interference and so on provided by photonics [9]–[11]. Until now, various photonics-based radar systems have been reported [12]–[26], which have shown remarkable superiority in the field of broad bandwidth, fast processing, and high resolution.

Several photonics-assisted approaches have been proposed to achieve dual-band processing. De-chirp is one typical pulse compression method to process with the linear frequency modulated (LFM) signals in radar systems. The dual-band receivers with de-chirp processing have been proposed in [21]–[23]. In [21], a dual-polarization quadrature phase shift keying (DP-QPSK) modulator consisting of two QPSK modulators along two orthogonal polarization axes is applied. The reference signals of the two bands are modulated to one QPSK modulator, while the echoes of the two bands are modulated to the other. The reference and the echo signals in one band are modulated to the optical carrier with the peak biasing points, while those in the other band are modulated with the null biasing points. By using the polarization de-multiplexing, the de-chirped outputs of the two bands can be obtained. Since the echoes from the two bands need to be modulated with different biasing points, thus they need to inject into different RF ports to be processed. Thus the processed RF signals are limited to two. In [22], specially designed dual-band LFM signals with inverse chirp rates are used to realize the dual-band photonic de-chirp processing. A photonic in-phase/quadrature (I/Q) mixing is introduced to distribute the two de-chirped output signals in different bands in the positive and negative spectrum, respectively. In [23], a dual-band transceiver with de-chirp processing based on photonics is proposed. In the transmitter, two optically carried LFM signals generated by photonic digital-to-analog conversion are mixed with an optical LO signal to the required RF bands and separated by two electrical band-pass filters. In the receiver, the dual-band echoes are de-chirped using a polarization multiplexing dual-drive MZM (PM-DMZM), which consists of two sub-DMZMs along two orthogonal polarization axes. The reference signal

and echo in one band are modulated at the two RF ports of one sub-DMZM, while those in the other band are modulated to the other sub-DMZM. Based on the polarization de-multiplexing technique, the dual-band echoes are jointly de-chirped and output, respectively. For the approaches in [21]–[23], the processing function is limited to the de-chirp method, and the processed RF signals are limited to two.

In [24], [25], a photonics-assisted multi-band radar transceiver is realized, for which the processing function is not limited to the de-chirp method. A mode-locked laser (MLL) is used as a shared unit to provide the multiple photonic LOs for the transmitter and the optical pulse source for the receiver. For the transmitting process, an electrical IF signal is modulated to the MLL source and then injected into a PD to realize the optical-to-electrical conversion. The RF signals with different center frequencies will be generated, which are then selected using electrical filters. In the receiver, the optical pulse source from the MLL is used to realize the optical sampling of the multi-band RF echo signals [24], or served as the multiple photonic LOs to downconvert the multi-band RF echo signals [25]. To realize the fine tuning of the carrier frequencies of the generated RF signals, the pulse repetition rate of the MLL is usually required to be small (e.g., 400 MHz). It leads to the strict requirement with either the optical filters to select the photonic LOs, or the electrical filters to select the needed RF signals. Besides, the IF signals downconverted from different bands need to locate at different frequencies to avoid the overlapping. Recently, a photonics-based dual-band receiver is proposed based on the photonic image-reject mixing and polarization multiplexing in [26]. By introducing two optical local oscillators (LOs) and two photonic image-reject mixers (IRMs) with two orthogonal polarization states, respectively, the two-band signals are downconverted to the same IF band simultaneously. Only the processing function is achieved, and the processed RF signals are also limited to two. For the previously proposed approaches, working simultaneously within two bands has been demonstrated (e.g., the processing in the C and Ku bands in [21], in the S and C bands in [22], in the X and Ku bands in [26], the signal generation and processing in the S and X bands in [24], [25]).

In this paper, we propose and demonstrate a multi-band transceiver based on polarization multiplexed photonic LOs and photonic mixers. Both for the multi-band transmitter and receiver sections, the polarization multiplexed photonic LO unit is shared, and the dual-polarization photonic mixer modules with similar structures are introduced. In this way, the architectural complexity is reduced, bringing benefits to the reliability, dimensions, and cost of the system. Based on the same transceiver, RF signals in four bands can be simultaneously generated, and the four-band RF echoes can be processed to the same IF band with interference effectively suppressed. The strict requirements with either the photonic or the electrical filters are avoided. Furthermore, the generation and processing capability of the proposed transceiver can be extended to being with $4N$ RF signals by introducing a polarization orthogonal optical frequency comb (OFC). Theoretical analyses are carried out, and a proof-of-concept experiment is taken. Four RF signals covering X, Ku, K and Ka bands with 1-GHz instantaneous bandwidth
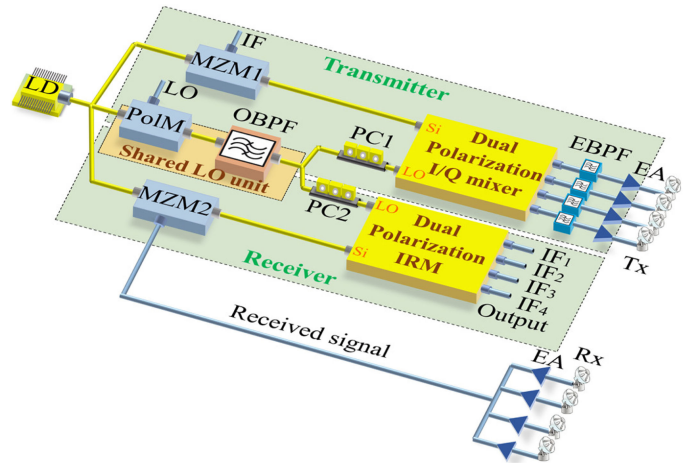

Fig. 1. The schematic diagram of the proposed photonics-based multi-band transceiver based on the polarization multiplexed photonic LOs and mixers. LD: laser diode; PolM: polarization modulator; OBPF: optical bandpass filter; MZM: Mach-Zehnder modulator; PC: polarization controller; EBPF: electrical bandpass filter; EA: electrical amplifier; I/Q: in-phase/quadrature; IRM: image-reject mixer.

are simultaneously generated, and the RF echoes are processed to the same IF band. The in-band crosstalk suppression ratio is larger than 26 dB for all the four bands. The ranging operated in K- and Ka-bands simultaneously are also implemented.

II. PRINCIPLE

Fig. 1 shows the schematic diagram of the proposed photonics-based multi-band transceiver. It is mainly composed of the polarization orthogonal photonic LOs, one dual-polarization photonic I/Q mixer, and one dual-polarization photonic IRM based on 90° optical hybrids. For the signal transmitting process, the polarization orthogonal photonic LOs and the dual-polarization photonic I/Q mixer are used. The dual-polarization photonic I/Q mixer is implemented by a polarization multiplexed 90° optical hybrid and four balanced photodetectors (BPDs). The IF signal is modulated to the optical carrier at MZM1 with the carrier suppressed double sideband (CS-DSB) modulation format. The modulated optical signal is then injected into the signal port of the polarization multiplexed 90° optical hybrid, while the photonic LOs with orthogonal polarization states are injected into the LO port. The dual-polarization photonic I/Q mixer module realizes the mixing between the optically carried IF signal and the two polarization orthogonal photonic LOs, respectively. With each photonic LO, two RF signals can be output through the up-conversion of the $\pm 1^{\text{st}}$ optically-carried IF sidebands. In this way, four RF signals can be generated with two polarization orthogonal photonic LOs.

For the signal processing, the received multi-band RF echo signals are first modulated to the optical carrier via MZM2 with the CS-DSB modulation format. The modulated optical signal is then injected into the signal port of the dual-polarization photonic IRM module, which is consisted of a polarization multiplexed 90° optical hybrid, four BPDs, and two electrical quadrature couplers. The two photonic LOs with orthogonal
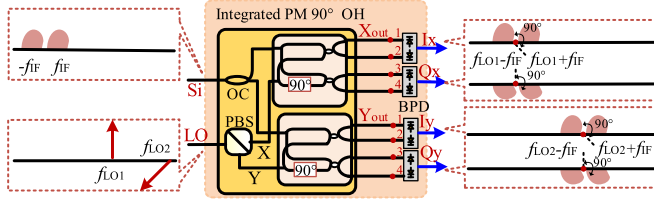
Fig. 2. The detailed structure of dual-polarization photonic I/Q mixer and the illustrations of the optical spectra at different points in the transmitter module. Integrated PM 90° OH: integrated polarization multiplexed 90° optical hybrid; BPD: balanced photodetector; PBS: polarization beam splitter; OC: optical coupler.

polarization states are injected into the LO port of the dual-polarization photonic IRM module. With each photonic LO, the echo signals in two bands located at the left and right sides of the photonic LO can be simultaneously down-converted. Thus with two polarization orthogonal photonic LOs, the downconversion of four-band RF signals can be achieved simultaneously.

For the polarization orthogonal photonic LOs generation in the shared photonic LO unit, a continuous wave (CW) light with a frequency of f_0 from a laser diode (LD) is injected into a polarization modulator (PolM), which is driven by a single-tone LO signal with a frequency of f_{LO}. An optical bandpass filter (OBPF) is applied after the PolM to select the $+1^{st}$ and the $+2^{nd}$ optical sidebands along two orthogonal polarization axes, which can be expressed as

$$\begin{bmatrix} E_{LO1}(t) \\ E_{LO2}(t) \end{bmatrix} = \left\{ \begin{matrix} \eta_1 \exp[j2\pi(f_0 + f_{LO1})t] \\ \eta_2 \exp[j2\pi(f_0 + f_{LO2})t] \end{matrix} \right\} \quad (1)$$

where $f_{LO1} = f_{LO}$, $f_{LO2} = 2f_{LO}$, η_1, η_2 are the amplitudes of the selected two sidebands, respectively. In this way, two photonic LOs with orthogonal polarization states are generated.

A. Multi-Band RF Signal Generation

In the transmitter, one part of the CW light from the same LD is sent to MZM1 biased at the minimum transmission point, at which an IF signal with a frequency of f_{IF} is modulated. The optical output of MZM1 can be expressed as

$$\begin{aligned} E_{IF}(t) &\propto \sin[\beta \cos(2\pi f_{IF}t)] \exp(j2\pi f_0 t) \\ &\approx J_1(\beta) \exp[j2\pi(f_0 - f_{IF})t] + J_1(\beta) \exp[j2\pi(f_0 + f_{IF})t] \end{aligned} \quad (2)$$

where β is the modulation index, and $J_1(\cdot)$ is the 1st-order Bessel function of the first kind. Considering the small-signal modulation format, high-order sidebands can be ignored and only two $\pm 1^{st}$-order sidebands are considered.

The obtained optically carried IF signal in Eq. (2) is injected into the signal port of the dual-polarization photonic I/Q mixer, while the two polarization orthogonal photonic LOs at $f_0 + f_{LO1}$ and $f_0 + f_{LO2}$ in Eq. (1) are sent into the optical LO port. The detailed structure of the dual-polarization photonic I/Q mixer module and the illustrations of the optical spectra at different positions are shown in Fig. 2. The dual-polarization I/Q mixer module is composed of an integrated polarization multiplexed 90° optical hybrid and four BPDs. The two polarization orthogonal photonic LOs are separated and output

at the two ports of the polarization beam splitter (PBS) and sent to the two 90° optical hybrids with orthogonal polarization states, respectively. Meanwhile, the optically carried IF signal is divided into two parts and sent to the two 90° optical hybrids. The photonic output signals of the dual-polarization 90° optical hybrids can be written as

$$\begin{cases} \begin{bmatrix} X_{out1}(t) \\ X_{out2}(t) \\ X_{out3}(t) \\ X_{out4}(t) \end{bmatrix} = \begin{bmatrix} 1 & 1 \\ 1 & -1 \\ 1 & j \\ 1 & -j \end{bmatrix} \begin{bmatrix} E_{IF}(t) \\ E_{LO1}(t) \end{bmatrix} \\ \begin{bmatrix} Y_{out1}(t) \\ Y_{out2}(t) \\ Y_{out3}(t) \\ Y_{out4}(t) \end{bmatrix} = \begin{bmatrix} 1 & 1 \\ 1 & -1 \\ 1 & j \\ 1 & -j \end{bmatrix} \begin{bmatrix} E_{IF}(t) \\ E_{LO2}(t) \end{bmatrix} \end{cases} \quad (3)$$

By sending the signals in Eq. (3) into four BPDs as shown in Fig. 2, respectively, two pairs of up-converted RF signals can be obtained as follows

$$\begin{cases} \begin{bmatrix} I_X \\ Q_X \end{bmatrix} = \begin{bmatrix} |X_{out1}(t)|^2 - |X_{out2}(t)|^2 \\ |X_{out3}(t)|^2 - |X_{out4}(t)|^2 \end{bmatrix} \\ \propto \eta_1 \begin{bmatrix} \cos[2\pi(f_{LO1} - f_{IF})t] + \cos[2\pi(f_{LO1} + f_{IF})t] \\ -\sin[2\pi(f_{LO1} - f_{IF})t] - \sin[2\pi(f_{LO1} + f_{IF})t] \end{bmatrix} \\ \begin{bmatrix} I_Y \\ Q_Y \end{bmatrix} = \begin{bmatrix} |Y_{out1}(t)|^2 - |Y_{out2}(t)|^2 \\ |Y_{out3}(t)|^2 - |Y_{out4}(t)|^2 \end{bmatrix} \\ \propto \eta_2 \begin{bmatrix} \cos[2\pi(f_{LO2} - f_{IF})t] + \cos[2\pi(f_{LO2} + f_{IF})t] \\ -\sin[2\pi(f_{LO2} - f_{IF})t] - \sin[2\pi(f_{LO2} + f_{IF})t] \end{bmatrix} \end{cases} \quad (4)$$

After being filtered, four RF signals can be generated as follows

$$\begin{cases} i_1(t) = \eta_1 \cos[2\pi(f_{LO1} - f_{IF})t] \\ i_2(t) = -\eta_1 \sin[2\pi(f_{LO1} + f_{IF})t] \\ i_3(t) = \eta_2 \cos[2\pi(f_{LO2} - f_{IF})t] \\ i_4(t) = -\eta_2 \sin[2\pi(f_{LO2} + f_{IF})t] \end{cases} \quad (5)$$

Due to the polarization orthogonal characteristics, two photonic LOs can be easily separated to avoid the strict requirement on the optical or electrical filters. By properly selecting the value of f_{LO} and f_{IF}, four RF signals within different bands can be generated.

B. Multi-Band Signal Downconversion

In the receiver, the RF echo signals are collected by the receiving antennas, amplified by electrical amplifiers (EAs), coupled together, and then modulated to the optical carrier at MZM2, as shown in Fig. 1. The illustration of the optical spectrum at the output of MZM2 (point a) is shown in Fig. 3, which is injected into the signal port of the dual-polarization photonic IRM. The two polarization orthogonal photonic LOs are injected into the LO port of the dual-polarization photonic IRM, with the spectrum illustration shown in Fig. 3(b). The dual-polarization IRM is composed of an integrated polarization multiplexed 90° optical hybrid, four BPDs, and two electrical quadrature couplers, as shown in Fig. 3. The two polarization orthogonal photonic LOs are separated and injected into the LO
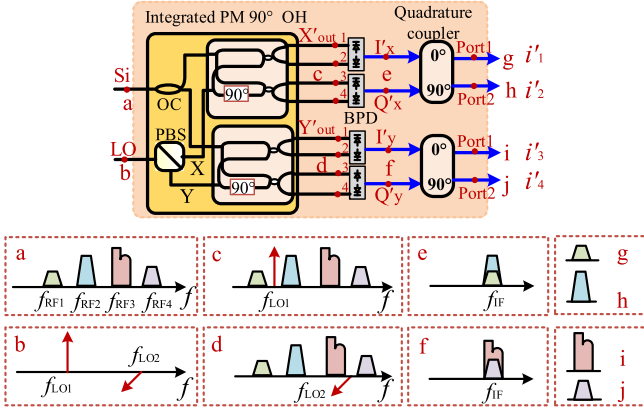
Fig. 3.   The detailed structure of the dual-polarization IRM in the receiver module. Insets: the illustration of the optical/electrical spectra at the corresponding points (a)-(j) in the dual-polarization IRM.

ports of the two 90° optical hybrids with orthogonal polarization states, respectively. The optically carried RF echo signal is equally power divided and injected into the signal ports of the two 90° optical hybrids, respectively. The spectrum illustrations of the optical signals at the outputs of the two 90° optical hybrids are shown in Figs. 3(c) and (d), respectively. Each 90° optical hybrid, in combination with two BPDs and an electrical quadrature coupler, form a photonic IRM based on the balanced Hartley structure [27]. In this way, the four-band RF signals are down-converted through the dual-polarization photonic IRMs.

Since the photonic IRMs with orthogonal polarization states are based on the same principle, here the photonic IRM with the X-polarization state is taken as an example to illustrate the principle for the downconversion of the RF signals in two bands. Mathematically, the optically carried RF echo signal and the photonic LO sent to the 90° optical hybrid with the X-polarized state are written as

$$\begin{cases} E_{\mathrm{RF}}(t) \propto \exp(j2\pi f_0 t) \begin{bmatrix} \kappa_1 \exp(j2\pi f_{\mathrm{RF1}}t) \\ +\kappa_2 \exp(j2\pi f_{\mathrm{RF2}}t) \\ +\kappa_3 \exp(j2\pi f_{\mathrm{RF3}}t) \\ +\kappa_4 \exp(j2\pi f_{\mathrm{RF4}}t) \end{bmatrix} \\ E_{\mathrm{LO1}}(t) = \eta_1 \exp[j2\pi(f_0 + f_{\mathrm{LO1}})t] \end{cases} \quad (6)$$

where $\kappa_{1,2,3,4}$ are the amplitudes of the $+1^{\mathrm{st}}$ sidebands of the optically carried RF echo signals in four bands, and $f_{\mathrm{RF1,2,3,4}}$ are the frequencies of the received RF signals in different bands, respectively. Since the mixing spurs between the photonic LO and the -1st optically carried RF echo sidebands are located far beyond the IF band, only the $+1^{\mathrm{st}}$ sideband is considered here. The four optical outputs of the X-polarized 90°optical hybrid are as follows

$$\begin{bmatrix} X'_{\mathrm{out1}}(t) \\ X'_{\mathrm{out2}}(t) \\ X'_{\mathrm{out3}}(t) \\ X'_{\mathrm{out4}}(t) \end{bmatrix} \propto \begin{bmatrix} 1 & 1 \\ 1 & -1 \\ 1 & j \\ 1 & -j \end{bmatrix} \begin{bmatrix} E_{\mathrm{RF}}(t) \\ E_{\mathrm{LO1}}(t) \end{bmatrix} \quad (7)$$

The two in-phase optical outputs ($X'_{\mathrm{out1}}, X'_{\mathrm{out2}}$) and the two quadrature optical outputs ($X'_{\mathrm{out3}}, X'_{\mathrm{out4}}$) in (7) are injected into

two BPDs, as shown in Fig. 3, respectively, with the electrical IF outputs as

$$\begin{bmatrix} I'_{\mathrm{X}} \\ Q'_{\mathrm{X}} \end{bmatrix} \propto \begin{bmatrix} |X'_{\mathrm{out1}}(t)|^2 - |X'_{\mathrm{out2}}(t)|^2 \\ |X'_{\mathrm{out3}}(t)|^2 - |X'_{\mathrm{out3}}(t)|^2 \end{bmatrix}$$

$$= \begin{bmatrix} \cos 2\pi(f_{\mathrm{LO1}} - f_{\mathrm{RF1}})t + \cos 2\pi(f_{\mathrm{RF2}} - f_{\mathrm{LO1}})t \\ -\sin 2\pi(f_{\mathrm{LO1}} - f_{\mathrm{RF1}})t + \sin 2\pi(f_{\mathrm{RF2}} - f_{\mathrm{LO1}})t \end{bmatrix} \quad (8)$$

By injecting the electrical outputs in (8) to an electrical quadrature coupler, the two outputs will be as follows

$$\begin{bmatrix} i'_1 \\ i'_2 \end{bmatrix} \propto \begin{bmatrix} j & 1 \\ 1 & j \end{bmatrix} \begin{bmatrix} I'_{\mathrm{X}} \\ Q'_{\mathrm{X}} \end{bmatrix} = \begin{bmatrix} -2\sin 2\pi(f_{\mathrm{LO1}} - f_{\mathrm{RF1}})t \\ 2\cos 2\pi(f_{\mathrm{RF2}} - f_{\mathrm{LO1}})t \end{bmatrix} \quad (9)$$

It can be seen that the IF signals downconverted from the two bands ($f_{\mathrm{RF1}}, f_{\mathrm{RF2}}$) will be obtained at the two output ports of the electrical quadrature coupler, with the electrical spectra illustrated in Figs. 3(g) and (h), respectively. In this way, the in-band interference between the signals downconverted from band 1 (f_{RF1}) and band 2 (f_{RF2}) shown in Fig. 3(e) is effectively suppressed. Besides, it is worthy to note that the DC component and the low-frequency mixing spurs generated from the beating with each other of the optically carried multiple RF echoes, including $|f_{\mathrm{RF1}} - f_{\mathrm{RF2}}|$ and $|f_{\mathrm{RF3}} - f_{\mathrm{RF4}}|$, are rejected due to the balanced detection, which is very helpful to avoid the false targets. Similarly, with the photonic LO and the photonic IRM with the Y-polarization state, the received RF echo signals in band 3 (f_{RF3}) and band 4 (f_{RF4}) will be downconverted and output from the two ports of the other electrical quadrature coupler, as illustrated in Figs. 3(i) and (j), respectively. Thus based on the dual-polarization photonic IRM and the two polarization orthogonal photonic LOs, the received RF echo signals from four bands can be downconverted and output independently.

III. Experiment Results

Based on the schematic diagram shown in Fig. 1, an experiment is carried out with the setup shown in Fig. 4. A lightwave is generated from an LD (TeraXion Inc., NLL04), and the wavelength is set to be 1550.55 nm. The shared photonic LO unit is composed of a PolM (Versawave Technologies Inc., 40 Gb/s) and an OBPF (Yenista XTM-50). A microwave source (Agilent E8257D, 250 kHz-67 GHz) is utilized to provide the LO signal. In the transmitter, MZM1 (Fujitsu FTM7938EZ, 40-Gb/s) with a half-wave voltage of 3.5 V is used. The IF signal is generated by an arbitrary waveform generator (AWG, Tektronix AWG70000, 50 GSa/s). Limited by the available experimental devices, an optical coupler, a PBS, and two 40-GHz photodetectors (PDs, XPDV2120RA) with a responsivity of 0.65 A/W are used to approximately replace the "dual-polarization I/Q mixer" module. In the receiver, MZM2 (Fujitsu FTM7938EZ, 40-Gb/s) with a half-wave voltage of 3.5 V is used. For the dual-polarization photonic IRM unit, an integrated polarization multiplexed 90° optical hybrid (Kylia COH28), two BPDs (BPDV2150R-VF-FP) with a 3-dB bandwidth of 40 GHz and an electrical quadrature hybrid (PULSAR QSB-13-463-7S, 0.5–10 GHz) are used. Optical tunable delay lines (OTDL, General Photonics) with 0~600ps continuous tuning range are connected
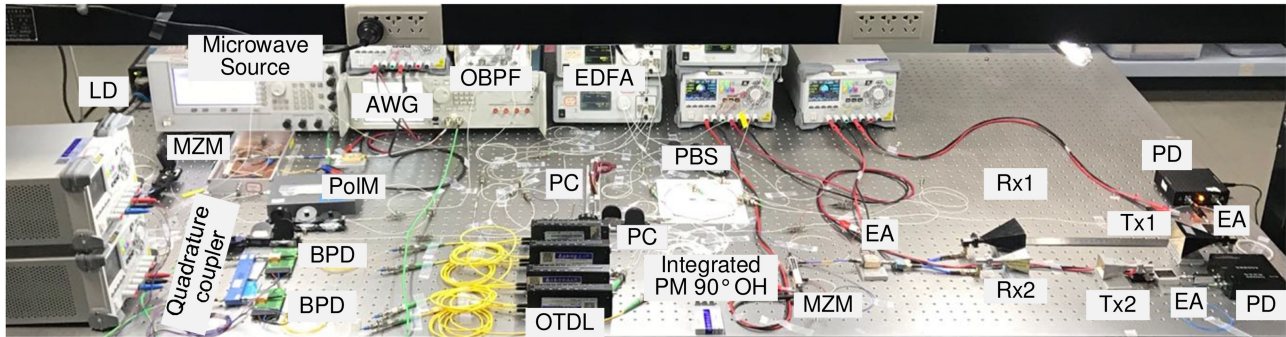
Fig. 4. The experimental setup of the photonics-based transceiver based on polarization multiplexed photonic LOs and mixers. AWG: arbitrary waveform generator; PD: photodetector; EDFA: erbium-doped fiber amplifier; OTDL: optical tunable delay liner.
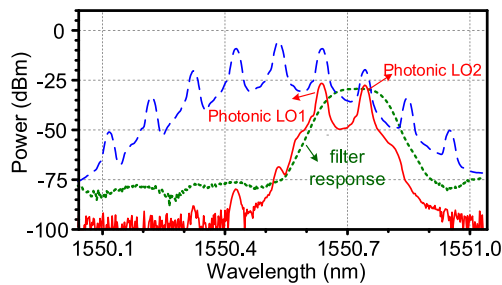

Fig. 5. Experimentally measured optical spectra of the signals at the output of the PolM (blue dashed line), the transmission response of the OBPF following the PolM (green dotted line), and the output of the OBPF (red solid line).
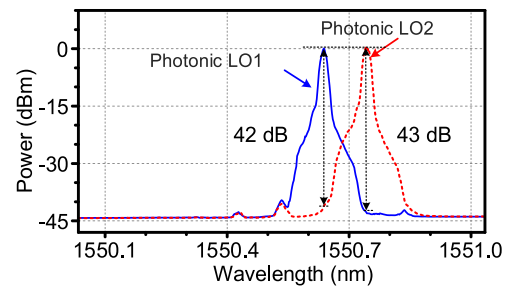

Fig. 6. The optical spectra of the orthogonally polarized output with the two photonic LOs.

to the output ports of the 90° optical hybrids. They are used for compensating the path imbalances due to the use of the discrete devices in the experiments. The optically-carried IF signal, the optically-carried RF signal and the shared photonic LO signal are amplified by three EDFAs (Amonics, AEDFA-PA-35-B-FA), respectively. An optical spectrum analyzer (YOKOGAWA AQ6370C, 0.02-nm resolution) and an electrical spectrum analyzer (R&SFSV40, 10 Hz-40 GHz) are adopted to observe the optical and electrical spectra, respectively.
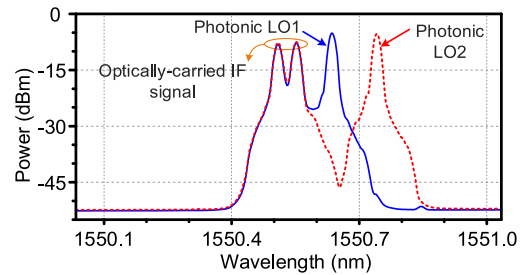

Fig. 7. The optical spectra of the output from the two ports of the PBS after passing the coupled optical signal through a PC followed by a PBS (the output of one port in blue solid line; the output of the other port in red dotted line).

A. The Photonic LOs Generation

In the shared photonic LO unit, the PolM is driven by a 13-GHz single-tone LO signal. The optical spectrum at the output of the PolM is shown as the blue dashed line in Fig. 5. An OBPF with the transmission response shown as the green dotted line in Fig. 5 is used to select the $+1^{st}$ and $+2^{nd}$ modulated optical sidebands. In this way, two orthogonal photonic LOs are generated, with the spectrum shown as the red solid line in Fig. 5.

To verify that the photonic LOs are along two orthogonal polarization axes, the output of the OBPF following the PolM is injected into the LO port of the integrated polarization multiplexed 90°optical hybrid via a PC. The optical spectra of the two orthogonally polarized signals at the two output ports of the polarization orthogonal 90° optical hybrids are shown in Fig. 6. It can be seen that the two photonic LOs are indeed orthogonal with the polarization isolation ratio of more than 40 dB.

B. Multi-Band Signal Generation

For the multi-band RF signal generation, an IF-LFM signal centered at 2.7 GHz with a bandwidth of 1 GHz and a time width of 2 µs is applied to the RF port of MZM1. The optically-carried IF signal is coupled with the photonic LOs. After passing through a PC followed by a PBS, the optical signal components with orthogonal polarization states are separated and output from the two ports of the PBS. The optical spectra are shown as the blue solid line and the red dotted line in Fig. 7, respectively. By injecting the two outputs into two PDs, RF signals are obtained, with the electrical spectra shown in Figs. 8(a) and (b), respectively. As can be seen, two RF signals with the frequency covering 9.8–10.8 GHz (X-band) and 15.2–16.2 GHz (Ku-band) are generated with the optical output with one polarization state. Besides, two RF signals with the frequency covering
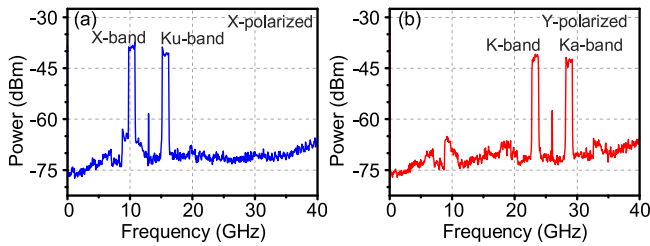
Fig. 8. The experimentally obtained electrical spectra at the PD outputs with the optical signals with the spectra (a) in blue solid line and (b) in the red dotted line shown in Fig. 7.
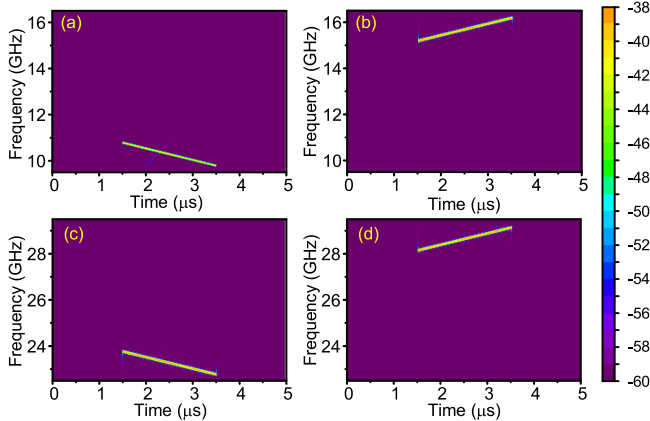

Fig. 9. The instantaneous frequency-time diagrams of the generated four RF-LFM signals with the frequency covering (a) X-band: 9.8–10.8 GHz; (b) Ku-band: 15.2–16.2 GHz; (c) K-band: 22.8–23.8 GHz; (d) Ka-band: 28.2–29.2 GHz.

22.8–23.8 GHz (K-band) and 28.2–29.2 GHz (Ka-band) are also obtained with the optical output with the other orthogonal polarization state. It should be mentioned that the spurs at 13 and 26 GHz can be observed in Figs. 8(a) and (b), respectively, which are the LO leakages. It is mainly caused by the non-ideal carrier suppressed double sideband modulation at the MZMs. The spur suppression ratio can be further improved by using MZMs with higher extinction ratios.

By using electrical bandpass filters, four RF signals covering from X to Ka bands are obtained, with the instantaneous frequency-time diagrams shown in Figs. 9(a)–(d), respectively. Here the LO leakages are also efficiently suppressed simultaneously. As can been seen, about 20-dB signal-to-clutter ratios are obtained for all the four RF signals. The four LFM signals are the pulse signals with the duty ratio of 50%, which is determined by the input IF signal function. It should be noted that the obtained RF signals in Figs. 9(a) and (c) are down-chirped, while the obtained RF signals in Figs. 9(b) and (d) are up-chirped. This is due to the symmetry of the $\pm 1^{\text{st}}$ IF sidebands about the optical carrier.

C. Multi-Band Signal Downconversion With the Spurs Suppression

For the multi-band RF signal downconversion, the performance of the multi-band image reject mixing is firstly investigated. Two groups of RF signals being the image for each other
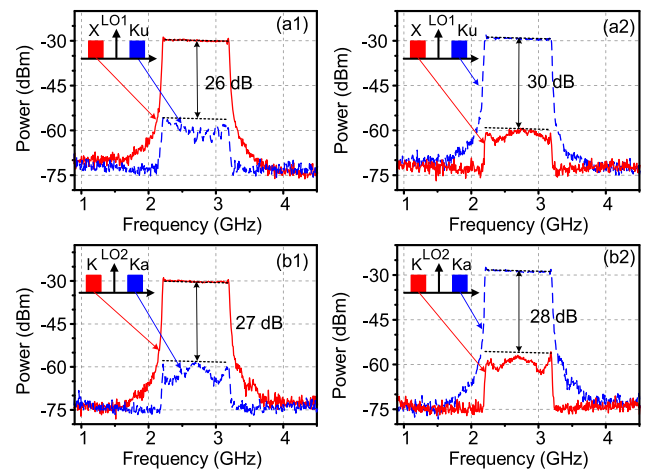

Fig. 10. The down-converted IF signals at the output (1) port 1 and (2) port 2 of the quadrature coupler in the (a) X-polarized and (b) Y-polarized path when four-band RF signals are applied one by one.

are employed as the received signals. Two RF signals covering 9.8–10.8 GHz in the X band and 15.2–16.2 GHz in the Ku band, are applied to the RF port of MZM2. For photonic LO1, the two optically carried RF signals act as the image for each other. The RF signals are down-converted to the same IF band and output from the two ports of the electrical quadrature coupler, respectively, with the electrical spectra shown in Figs. 10(a1) and (a2), respectively. The two red solid lines represent the IF signals output at the two ports of the electrical quadrature coupler when only the X-band RF signal is applied, while the two blue dashed lines represent those when the Ku-band RF signal is applied. The crosstalk suppression ratio between the desired IF signal and the corresponding image component is larger than 26 dB. Similarly, the other group of RF signals, consisting of a K-band signal covering 22.8–23.8 GHz and a Ka-band signal covering 28.2–29.2 GHz, are also down-converted by photonic LO2 with the Y polarization state. The electrical spectra of the down-converted IF signals are illustrated in Figs. 10(b1) and (b2), respectively. The two red solid lines represent the IF signal output at the two ports of the electrical quadrature coupler when the K-band RF signal is applied, while the blue dashed lines represent those when the Ka-band RF signal is injected. As can be seen, the simultaneous downconversion of two RF signals with a crosstalk suppression ratio of larger than 27 dB is also successfully achieved. In this way, with one dual-polarization photonic IRM unit, the downconversion of the RF signals in four bands with a large crosstalk suppression ratio can be obtained.

Since the photonic LOs are separated through the PBS, thus the good polarization isolation ratio guarantees the good in-band crosstalk suppression ratio. To investigate the in-band crosstalk suppression ratio performance, a two-tone signal with frequencies of 15.5 GHz (Ku band) and 29 GHz (Ka band) is applied. The downconversion result of the Ku-band signal with photonic LO1 with the X-polarization state is shown in Fig. 11(a). As can be seen, the needed IF signal at 2.5 GHz and a spur at 3 GHz exist. The spur is generated from the mixing between the leakage of photonic LO2 and the optically carried 29-GHz Ka-band
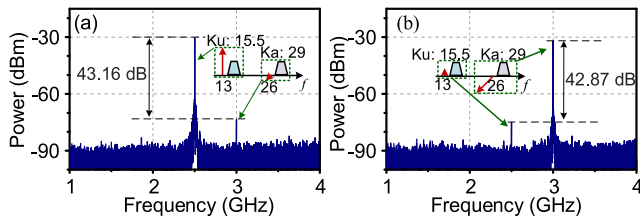
Fig. 11. The electrical spectra of the down-converted IF signals at the output port 2 of the quadrature coupler in the (a) X-polarized and (b) Y-polarized path when the 15.5-GHz (Ku band) and 29-GHz (Ka band) signals are applied simultaneously.
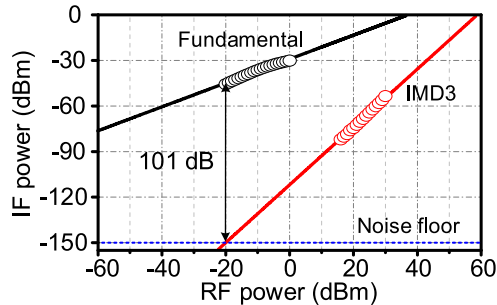

Fig. 12. The experimentally measured spurious-free dynamic range (SFDR) performance of the photonic IRM receiving module with the X-polarization state.
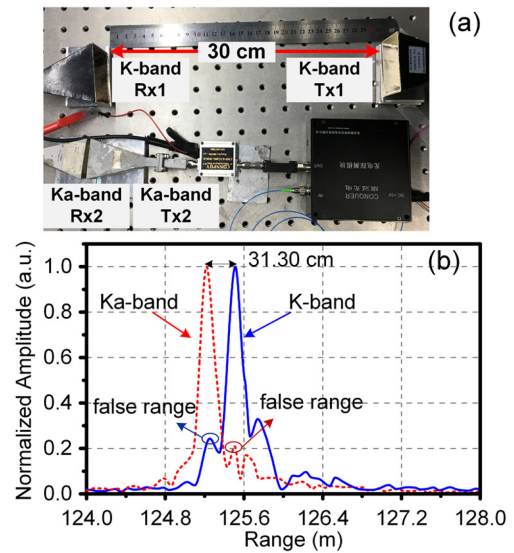

Fig. 13. (a) Configuration for the range detection operating in the K and Ka bands based on the proposed transceiver, (b) the cross-correlation results between the input IF-LFM waveform and the obtained IF-LFM waveform downconverted from K band (blue solid line) and Ka band (red dotted line).

signal. The downconversion result of the Ka-band signal with photonic LO2 is shown in Fig. 11(b). Not only the needed IF signal at 3 GHz but also the crosstalk at 2.5 GHz exist, which generates from the mixing of the leaked photonic LO1 with the optically carried Ku-band signal. The crosstalk suppression ratio is larger than 42.8 dB for both cases, which agrees well with the polarization isolation ratio of the two photonic LOs shown in Fig. 6.

To further investigate the proposed receiver module performance, the spurious-free dynamic range (SFDR) is also measured experimentally with the photonic IRM receiving module with the X-polarization state. A two-tone RF signal with the frequencies of 16.50 and 16.52 GHz is introduced, and the LO signal applied to the PolM is set to be 15 GHz. The measured SFDR is about 101 dB·Hz$^{2/3}$ when the noise floor is assumed to be -150 dBm/Hz, as shown in Fig. 12.

For practical applications in radar systems, further improvements need to be carried out with the performances, especially the crosstalk suppression ratio. As mentioned above, the in-band interference is mainly caused by the image and the polarization crosstalk. Precious designs of the 90° optical hybrid and the accurate control of the polarization state can lead to a better performance [28].

D. Dual-Band Ranging

To further investigate the performance of the proposed photonics-based multi-band transceiver, a dual-band ranging experiment is taken in the lab. A K-band LFM signal covering 22.8–23.8 GHz and a Ka-band LFM signal covering 28.2–29.2

GHz are generated by using photonic LO2 and the input IF-LFM signal covering 2.2–3.2 GHz in the proposed transmitter, as shown in Figs. 9(c) and (d). After being amplified by the EAs, these RF signals are emitted via the K-band antenna (Tx1) and the Ka-band antenna (Tx2), respectively. Receiving antennas are placed back-to-back with the distances of ∼30 cm and ∼0 cm away from the corresponding transmitting antennas, respectively, as shown in Fig. 13(a). The two RF signals collected by the receiving antennas are amplified by EAs, coupled together, and injected into the RF port of MZM2. The two IF-LFM signals covering 2.2–3.2 GHz downconverted with photonic LO2 from the K- and Ka-bands are output from the two ports of the electrical quadrature coupler, respectively. The cross-correlation results between the reference IF signal and the down-converted IF signals in the receiver are shown in Fig. 13(b). The red dotted line is related to the Ka-band signal and the blue solid line is related to the K-band signal. By measuring the peak positions of the cross-correlation results, a distance of 31.3 cm can be calculated out, which agrees well with the 30-cm distance between the K-band emitting antenna and the receiving antenna. Besides, as can be seen from Fig. 13(b), the false ranges caused by the image interferences are greatly suppressed. Thus the multi-band RF signals generation and the simultaneous processing of the multiple-band RF echo signals with large interference suppression is verified based on the proposed microwave photonic transceiver.

IV. DISCUSSION

The generation and processing of the RF signals covering four bands have been achieved based on the proposed microwave photonic transceiver in the experiment. Furthermore, the working band number can be extended to $4N$ if an orthogonally polarized optical frequency comb (OFC) with $2N$ comb lines
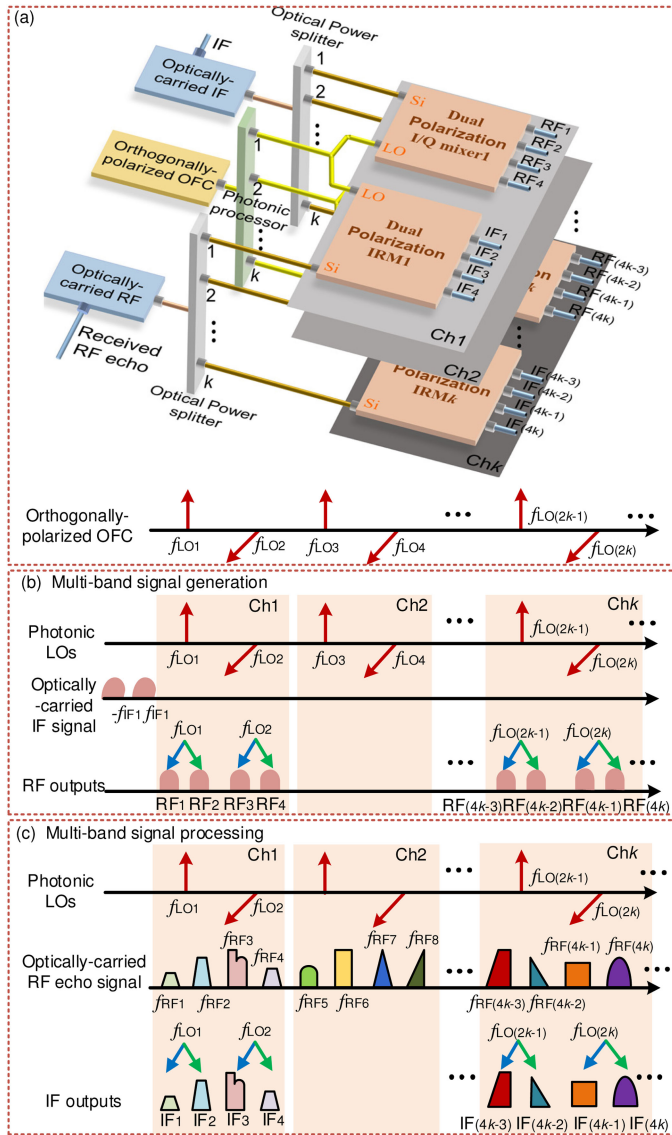
Fig. 14. (a) The schematic diagram to extend the capability of the proposed multi-band transceiver by introducing an orthogonally polarized OFC, inset: the spectrum illustration of the OFC. The principle illustrations of the multi-band signal (b) generation and (c) processing. OFC: optical frequency comb.

is used, as shown in Fig. 14(a). For the RF signals generation, as shown in Fig. 14(b), two adjacent comb lines along two orthogonal polarization axes with the frequencies of $f_{\mathrm{LO}(2k-1)}$ and $f_{\mathrm{LO}(2k)}$ ($k = 1, 2, \ldots, N$) are selected and injected to the LO port of the kth "dual-polarization photonic I/Q mixer". The IF signal injected to the system would be up-converted and four RF signals will be generated, which can be expressed as

$$\begin{cases} f_{\mathrm{RF}(4k-3)} = f_{\mathrm{LO}(2k-1)} - f_{\mathrm{IF}} \\ f_{\mathrm{RF}(4k-2)} = f_{\mathrm{LO}(2k-1)} + f_{\mathrm{IF}} \\ f_{\mathrm{RF}(4k-1)} = f_{\mathrm{LO}(2k)} - f_{\mathrm{IF}} \\ f_{\mathrm{RF}(4k)} = f_{\mathrm{LO}(2k)} + f_{\mathrm{IF}} \end{cases} \qquad (10)$$

In the receiver, the RF echo signals are collected and coupled together, and then injected into the RF port of MZM2. Then the optically carried RF echo signal and the corresponding photonic

LOs ($f_{\mathrm{LO}(2k-1)}$ and $f_{\mathrm{LO}(2k)}$) are sent to the signal port and the LO port of the kth "dual-polarization photonic IRM", respectively, as illustrated in Fig. 14(a). The RF echo signals will be down-converted and output with effective crosstalk suppression, as shown in Fig. 14(c). Thus in this way, by utilizing $2N$ polarization orthogonal photonic comb lines, N dual-polarization photonic I/Q mixers and N dual-polarization photonic IRMs, the generation and processing capability of the proposed transceiver can be extended to $4N$ RF signals.

For the proposed transceiver, the RF carrier frequencies can be adjusted flexibly by tuning the LO and IF carrier frequencies, and the waveform format can be also changed by adjusting the input IF waveform. On the other hand, the RF signals in different bands are obtained from the same IF signal, thus the RF signal formats in different bands are the same. In addition, the scheme forces the RF signal frequencies in different bands to obey a law depending on the LO and IF frequencies. These characteristics lead to the restrictions on the waveforms and the managed frequencies in different bands, which will be investigated in our future work.

V. CONCLUSION

In conclusion, a photonics-based multi-band RF transceiver is proposed and demonstrated. The shared polarization multiplexed photonic LO unit and the dual-polarization photonic mixer modules with similar structures are introduced both for the transmitter and the receiver sections. The architectural complexity is reduced, improving the reliability, dimensions, and cost of the system. Based on the same transceiver, RF signals in four bands can be simultaneously generated, and the four-band RF echoes can be processed to the same IF band with interference effectively suppressed. Furthermore, the generation and processing capability with $4N$ RF signals can be achieved with the proposed transceiver, when $2N$ polarization orthogonal comb lines, N dual-polarization photonic I/Q mixers, and N dual-polarization photonic IRMs are utilized. By introducing microwave photonic integration techniques, the OTDLs in the experiments can be removed to guarantee the simplicity of the system. In the proof of concept experiment, a photonics-based transceiver to generate and process four RF signals covering X, Ku, K and Ka bands with 1-GHz instantaneous bandwidth is successfully achieved. The proposed scheme can find applications in the future cognitive RF systems that need to work in multiple bands and have a variety of functions to learn, infer, and react to the environment.

REFERENCES

[1] S. Haykin, "Cognitive radar: A way of the future," *IEEE Signal Process. Mag.*, vol. 23, no. 1, pp. 30–40, Jan. 2006.
[2] J. Ender and S. Bruggenwirth, "Cognitive radar—Enabling techniques for next generation radar systems," in *Proc. IEEE 16th Int. Radar Symp.*, 2015, pp. 3–12.
[3] M. Vespe, C. J. Baker, and H. D. Griffiths, "Automatic target recognition using multi-diversity radar," *IET Radar Sonar Navigat.*, vol. 1, no. 6, pp. 470–478, 2007.
[4] D. Zhu and S. L. Pan, "Broadband cognitive radio enabled by photonics," *J. Lightw. Technol.*, vol. 38, no. 12, pp. 3076–3088, Jun. 2020.
[5] M. I. Skolnik, *Radar Handbook*. New York, NY, USA: McGraw-Hill, 2008.

[6] W. L. Melvin and J. A. Scheer, *Principles of Modern Radar: Advanced Techniques*. Rijeka, Croatia: Scitech, 2012.

[7] H. Darabi, A. Mirzaei, and M. Mikhemar, "Highly integrated and tunable RF front ends for reconfigurable multiband transceivers: A tutorial," *IEEE Trans. Circuits Syst. I, Reg. Papers*, vol. 58, no. 9, pp. 2038–2050, Sep. 2011.

[8] V. Vidojkovic, J. V. D. Tang, A. Leeuwenburgh, and A. V. Roermund, *Reconfigurable Multi-Band RF Front-End*. Berlin, Germany: Springer, 2008.

[9] J. D. Mckinney, "Technology: Photonics illuminates the future of radar," *Nature*, vol. 507. no. 7492, pp. 310–311, 2014.

[10] S. L. Pan, D. Zhu, and F. Z. Zhang, "Microwave photonics for modern radar systems," *Trans. Nanjing Univ. Aeronaut. Astronaut.*, vol. 31, no. 3, pp. 219–240, 2014.

[11] T. R. Clark and R. Waterhouse, "Photonics for RF front ends," *IEEE Microw. Mag.*, vol. 12, no. 3, pp. 87–95, May 2011.

[12] P. Ghelfi *et al.*, "A fully photonics-based coherent radar system," *Nature*, vol. 507, no. 7492, pp. 341–345, 2014.

[13] F. Z. Zhang *et al.*, "Photonics-based broadband radar for high-resolution and real-time inverse synthetic aperture imaging," *Opt. Express*, vol. 25, no. 14, pp. 16274–16281, Jun. 2017.

[14] X. W. Ye, F. Z. Zhang, Y. Yang, and S. L. Pan, "Photonics-based radar with balanced I/Q de-chirping for interference-suppressed high-resolution detection and imaging," *Photon. Res.*, vol. 7, no. 3, pp. 265–272, Mar. 2019.

[15] X. W. Ye, F. Z. Zhang, Y. Yang, D. Y. Zhu, and S. L. Pan, "Photonics-based high-resolution 3D inverse synthetic aperture radar imaging," *IEEE Access*, vol. 7, pp. 79503–79509, Jul. 2019.

[16] R. Li *et al.*, "Demonstration of a microwave photonic synthetic aperture radar based on photonic-assisted signal generation and stretch processing," *Opt. Express*, vol. 25, no. 13, pp. 14334–14340, Jun. 2017.

[17] A. Wang *et al.*, "Ka-band microwave photonic ultra-wideband imaging radar for capturing quantitative target information," *Opt. Express*, vol. 26, no. 16, pp. 20708–20717, Aug. 2018.

[18] S. Peng *et al.*, "High-resolution W-band ISAR imaging system utilizing a logic-operation-based photonic digital-to-analog converter," *Opt. Express*, vol. 26, no. 2, pp. 1978–1987, Jan. 2018.

[19] Q. S. Guo, F. Z. Zhang, P. Zhou, and S. L. Pan, "Dual-band LFM signal generation by frequency quadrupling and polarization multiplexing," *IEEE Photon. Technol. Lett.*, vol. 29, no. 16, pp. 1320–1323, Aug. 2017.

[20] W. J. Chen *et al.*, "Photonics-based reconfigurable multi-band linearly frequency-modulated signal generation," *Opt. Express*, vol. 26, no. 25, pp. 32491–32499, Dec. 2018.

[21] J. Cao *et al.*, "Photonic deramp receiver for dual-band LFM-CW radar," *J. Lightw. Technol.*, vol. 37, no. 10, pp. 2403–2408, May 2019.

[22] Z. Meng *et al.*, "Dual-band dechirping LFMCW radar receiver with high image rejection using microwave photonic I/Q mixer," *Opt. Express*, vol. 25, no. 18, pp. 22055–22065, Sep. 2017.

[23] S. Peng *et al.*, "A photonics-based coherent dual-band radar for super-resolution range profile," *IEEE Photon. J.*, vol. 11, no. 4, Aug. 2019, Art. no. 5502408.

[24] F. Scotti, F. Laghezza, P. Ghelfi, and A. Bogoni, "Multi-band software-defined coherent radar based on a single photonic transceiver," *IEEE Trans. Microw. Theory Tech.*, vol. 63, no. 2, pp. 546–552, Feb. 2015.

[25] P. Ghelfi, F. Laghezza, F. Scotti, D. Onori, and A. Bogoni, "Photonics for radars operating on multiple coherent bands," *J. Lightw. Technol.*, vol. 34, no. 2, pp. 500–507, Jan. 2016.

[26] J. Liu, D. Zhu, W. J. Chen, and S. L. Pan, "Photonics-based dual-band RF receiver with large crosstalk suppression," in *Proc. 10th Int. Conf. Inf. Opt. Photon.*, Jul. 8–11, 2018, pp. 109646M-1–109646M-4.

[27] D. Zhu, W. J. Chen, and S. L. Pan, "Photonics-enabled balanced Hartley architecture for broadband image-reject microwave mixing," *Opt. Express*, vol. 26, no. 21, pp. 28022–28029, Oct. 2018.

[28] W. J. Chen, D. Zhu, C. X. Xie, and S. L. Pan, "Image reject mixer with greatly improved rejection ratio based on the balanced Hartley architecture," in *Proc. 6th IEEE MTT-S Int. Wireless Symp.*, May 19–22, 2019, pp. 1–3.

Wenjuan Chen received the B.S. degree in electronic science and technology in 2016 from the Nanjing University of Aeronautics and Astronautics, Nanjing, China, where she is currently working toward the Ph.D. degree. Her research interests include photonic signal processing and photonics-based RF front-end.

Dan Zhu (Member, IEEE) received the B.S. and Ph.D. degrees in electronic engineering from Tsinghua University, Beijing, China, in 2004 and 2009, respectively. In May 2011, she joined the College of Electronic and Information Engineering, Nanjing University of Aeronautics and Astronautics, Nanjing, China, where she is currently a Professor. From May 2014 to May 2015, she was a Visiting Scholar at the Microwave Photonics Research Laboratory, University of Ottawa, Canada. Her current research interests include microwave photonic signal processing and the system applications.

Dr. Zhu is a member of the IEEE Microwave Theory and Techniques Society, the IEEE Photonics Society, and the Optical Society of America.

Jiang Liu received the B.S. degree in electronic science and technology in 2018 from the Nanjing University of Aeronautics and Astronautics, Nanjing, China, where he is currently working toward the M.S. degree. His research focuses on microwave photonic processing.

Shilong Pan (Senior Member, IEEE) received the B.S. and Ph.D. degrees in electronic engineering from Tsinghua University, Beijing, China, in 2004 and 2008, respectively. From 2008 to 2010, he was a "Vision 2010" Postdoctoral Research Fellow with the Microwave Photonics Research Laboratory, University of Ottawa, Canada. In 2010, he joined the College of Electronic and Information Engineering, Nanjing University of Aeronautics and Astronautics, China, where he is currently a Full Professor and an Executive Director of the Key Laboratory of Radar Imaging and Microwave Photonics, Ministry of Education.

He has authored or coauthored more than 420 research papers, including more than 240 papers in peer-reviewed journals and 190 papers in conference proceedings. His research focused on microwave photonics, which includes optical generation and processing of microwave signals, analog photonic links, photonic microwave measurement, and integrated microwave photonics.

Prof. Pan is currently an Associate Editor for *Electronics Letters*, a Topical Editor of *Chinese Optics Letters*, and is a Technical Committee Member of IEEE MTT-3 Microwave Photonics. He was also a Chair of a number of international conferences, symposia, and workshops, including the TPC Chair of the International Conference on Optical Communications and Networks in 2015, and TPC Co-Chair of the IEEE International Topical Meeting on Microwave Photonics in 2017. He is a Fellow of OSA, SPIE, and IET. He was selected as an IEEE Photonics Society Distinguished Lecturer in 2019.